CrossMark

Peer Reviewed

Effect of Heat Treatment on the Microstructure and Properties of HVOF-Sprayed Co-Cr-W Coating

Šárka Houdková, Eva Smazalová, and Zdeněk Pala

Co-Cr-W HVOF-sprayed protective coatings are used for their high oxidation and wear resistance. Apart from the oxidation resistance, the stability of their mechanical properties in relation to thermal loading is crucial with respect to the most common high-temperature application areas. This work is focused mainly on evaluation of the heat-induced changes in the phase composition and related mechanical properties. It was shown that the original powder, composed fully from face-centered cubic Co-based alloy, partly changes its phase composition during spraying to a hexagonal close-packed (hcp) structure. The annealing further increases the ratio of the hcp phase in the structure. The heat-induced phase changes are accompanied by an increase in the coatings' hardness and cohesion strength. The abrasive and adhesive wear behavior was evaluated. While the coatings' heat treatment had a positive effect on the coefficient of friction, the abrasive and adhesive wear resistance of annealed coating was lower compared to as-sprayed coating.

1. Introduction

Co-based alloys are well known for their excellent wear and corrosion properties. Depending on chemical composition, they offer different hardness, oxidation resistance over a wide range of temperature and other enhanced properties. The element content, as well as the technological treatment, is responsible also for the microstructure of the Co-based alloys (Ref 1).

Pure cobalt can exist in two allotropic modifications—the high-temperature fcc phase (usually denoted as α-Co) and the low-temperature hcp phase (denoted as either β-Co or ε-Co), with transformation temperature about 417 °C (Ref 2), strongly depending on purity. However, the free energy associated with phase transitions is low, i.e., 500 J/mol and 360 J/mol for hcp to fcc and fcc to hcp modifications (Ref 3), respectively. Therefore, in polycrystalline Co, the metastable fcc phase is usually present at room temperature, stabilized when the grain size is reduced (Ref 4). The metastable fcc phase is prone to stress-induced martensitic transformation during deformation due to the its low stacking fault energy (Ref

5, 6). This transformation is responsible for work hardening, one of the main sources of the high wear and erosion resistance of Co-based alloys. The transformation mechanisms of pure Co (Ref 2-5) and its Co-Cr-Mo alloys (Ref 6-13) were described in detail in various studies.

The choice of alloying elements is vital regarding the optimization of alloys' properties and microstructure. Chromium is responsible for high-temperature corrosion and oxidation resistance and contributes significantly to the strengthening of alloys through formation of M_7C_3 and $M_{23}C_6$ carbides and through creation of a solid solution. The Mo and W contents have a similar effect—the strengthening of the alloy by formation of carbides and intermetallic phases, or, in the case of low C content, the strengthening of the solid solution. The stability of the fcc phase even at room temperature is fostered by the addition of C, Ni and Fe. On the other hand, Cr, Mo and W tend to stabilize the hcp structure (Ref 14, 15).

Based on the carbon content, the Co-based alloy microstructure can be hypoeutectic, consisting of the Co-fcc primary dendrites surrounded by a network of carbides, or hypereutectic, with primary carbides and an interdendritic eutectic matrix (Ref 16). The role of carbides regarding wear resistance was studied extensively for Co-Cr-Mo biomedical alloys (Ref 10-13) and for Co-Cr-W industrial alloys (Ref 15-18). Nevertheless, the results of these studies are not in agreement: While some found carbides beneficial for wear resistance, the others consider them responsible for increasing wear through an abrasive mechanism during sliding (Ref 10, 11, 17). The influence of fcc to hcp transformation on the tribological performance was intensively studied only for the Co-Cr-Mo alloy, intended usually for biomedical applications (Ref 10-12). It was shown that a low-carbon alloy consisting only of an fcc Co-based solid solution is more prone

Šárka Houdková and **Eva Smazalová**, New Technologies Research Centre, University of West Bohemia, Univerzitní 22, 306 14 Plzeň, Czech Republic; and **Zdeněk Pala**, Institute of Plasma Physics, Czech Academy of Sciences, Za Slovankou 3, 182 00 Prague, Czech Republic. Contact e-mails: houdkov@ntc.zcu.cz, smazal@ntc.zcu.cz, and pala@ipp.cas.cz.

to a stress-induced fcc to hcp transformation during wear (Ref 10). The hcp structure is harder and less ductile and is believed to have higher wear resistance. Similar findings were published in (Ref 11). The low-carbon fcc phase had lower hardness due to the lack of carbides, but better wear resistance, thanks to the formation of a subsurface hcp layer in the wear track.

In surface engineering, the Co-Cr-W (commonly known as Stellite®) alloys are widely used as a protection against different kinds of wear, namely cavitation and erosion, corrosion and oxidation. Different deposition technologies can be used to deposit a Stellite layer onto the surface of parts, e.g., PTA welding, thermal spraying or laser cladding. The properties of coating vary according to the technology used, in consequence of microstructure difference. Numbers of studies were published regarding the laser-cladded Stellite (Ref 15, 16, 18-33). They include laser process parameters studies (Ref 19, 21, 24, 27, 32, 33), studies of the influence of substrate materials and conditions (Ref 24, 28, 30, 31, 33) and comparisons of Stellite coating deposited by different technologies (Ref 16, 20). The most detailed evaluation of microstructure and properties of laser-clad Stellite coatings was carried out by Ocelík et al. (Ref 20-27). Most of the studies reported that the microstructure of laser-clad Stellite coatings consisted of fcc Co-based dendrites surrounded by a net of $M_{23}C_6$ or M_7C_3 carbides. The morphology of carbides differs depending on the process parameters (Ref 15, 16) or the following heat treatment (Ref 20). The strain-hardening effect connected with fcc to hcp strain-induced transformation was not, according to the authors' best knowledge, described for Stellite coatings by any study.

In contrast to the comprehensive research on laser-clad coatings, less was published concerning thermally sprayed Stellite coatings. Primary attention was paid to HVOF-sprayed Stellite coatings by Sidhu et al. (Ref 14, 34-38). In his studies, in particular high-temperature oxidation and corrosion resistance were evaluated and compared to other types of coating material; a similar topic was addressed also in (Ref 39). Other researchers focused on the suitability of HVOF-sprayed Stellite coating for different applications and load conditions, namely cavitation and erosion wear (Ref 40-43). The microstructure of HVOF Stellite coating was analyzed in (Ref 14, 44); Zhang (Ref 44) reported on the fcc Co-rich phase with few Cr_7C_3 carbides, identified by XRD, but not visible by SEM. In the work of Sidhu (Ref 14), only a 100% fcc Co-based solid solution was investigated. The carbide precipitation is suppressed by a high cooling rate during the spraying process. The Stellite coatings are very often applied in a high-temperature environment. In addition to high oxidation resistance, the stability of mechanical properties is important as well. None of the above-mentioned studies evaluated the influence of high temperature on the HVOF-sprayed Stellite coatings' microstructure and wear resistance.

The aim of this work is to analyze the microstructure and phase composition of HVOF as-sprayed and heat-treated Stellite 6 coatings with respect to possible fcc to hcp transformation and carbide precipitation and to evaluate the influence of microstructure changes on the tribological performance. The possible degradation of coatings' functional properties as a result of exposure to high temperatures can be estimated based on the results obtained.

2. Experimental Setup

The thermally sprayed coating was deposited onto grit-blasted carbon steel substrates, with dimensions designed according to the requirements of each test—(40 × 30 × 5) mm for microstructure analyses, (25 × 25 × 5) mm for the ASTM G-133 test (ball-on-flat sliding wear) and (75 × 25 × 5) mm for the ASTM G-65 test (dry sand/rubber wheel). Prior to the spraying, the substrates were grit-blasted by alumina with 0.8-1 mm grain sizes (F22) to achieve roughness of Ra = 8, approximately. The FST 484.074 Stellite 6 Co-based alloy feedstock powder with nominal composition 28%Cr, 5%W, 1.2%C, 1%Si, Co-rest, gas-atomized, particle size range 20-53 μm, was used for spraying by the HP/HVOF TAFA JP5000 spraying gun in Výzkumný a zkušební ústav Plzeň s.r.o. (The Research and Testing Institute in Plzeň, Ltd). The spraying parameters are summarized in Table 1. The thicknesses of the sprayed coatings were 400 ± 20 μm.

The coated samples were annealed in the air atmosphere in a muffle furnace (LM 212), at 600 °C for 116 h, and cooled in air. The annealing temperature was chosen in respect of the intended application of the coating onto engineering component parts working at the environment of operational steam temperatures in a steam turbine, i.e., 580 °C. The time of the exposure was set to ensure the complete phase transformation in the coating, but avoid massive surface oxidation. The influence of time of exposure on the coatings' properties was previously tested (Ref 45). The non-coated parts of steel samples were protected against oxidation by oxidation-protective paint CONDURSAL Z 1100. The as-sprayed and annealed coatings were then analyzed in terms of microstructure, phase composition and tribological performance.

The microstructure of the coatings was evaluated on cross sections (ground and polished by automatic Leco grinding and polishing equipment) using optical microscope Nikon Epiphot 200, digital optical 3D microscope Hirox KH7700 and SEM Quanta 200 from FEI.

The coatings' phase composition was evaluated and compared by means of x-ray diffraction (XRD), using the D8 Discover powder diffractometer in Bragg-Brentano geometry with 1D detector and CoKα radiation (scanned

Table 1 Coatings deposition parameters

HVOF	TAFA JP5000
Oxygen	996 l/min
Fuel	277 l/h
Barrel length	150 mm
Spray distance	360 mm
Traverse speed	250 mm/s
Feed rate	46 g/min
Carrier gas	Nitrogen, 6.5 l/min
Offset	6
Number of passes	7

region from 20° to 100° 2θ with 0.03° 2θ step size and 96 s counting time per step). The obtained diffraction patterns were subjected to quantitative Rietveld analysis (Ref 46) performed in TOPAS 4.2, which uses the so-called fundamental parameters approach (Ref 47). In this manner, (1) the feedstock powder, (2) the surface in the as-sprayed state and (3) the surface of the annealed coating in the as-received and ground state were analyzed in order to identify the oxides formed in the surface oxide layer together with potential changes of phase composition inside the coatings.

The microhardness was measured on the ground surface of both as-sprayed and annealed coatings using the HV0.3 method. For each coating, at least 10 indents were done, and the average value is reported.

The microhardness depth-profiles were evaluated by HV0.3 measurement for both as-sprayed and annealed coatings. The indents were made in 50-μm distant steps, starting 50 μm above the coatings' surface. Three indents were made in each depth; the average value is reported.

The coatings' cohesion strength was investigated using the Vickers indentation method, developed for indentation fracture toughness evaluation (Ref 48). At least 7 Vickers indents (150 N load) were placed in the middle of the coatings' cross sections. The indents dimensions and the length of the created cracks were measured by optical microscope and compared.

The abrasive wear resistance was evaluated using the dry sand rubber-wheel test according to ASTM G65. Test parameters were as follows: 22 N load; Al_2O_3 abrasive media; AG 29 rubber counterpart; and 718 m total abrasive distance. The samples were weighted after each 143 m, and the weight loss was converted to volume loss using density values determined experimentally on free-standing coatings using the Archimedes principle. For FST 484.074 coating sprayed using parameters stated in Table 1, density of 8.296 g/cm^3 was used. The surface of both as-sprayed and annealed coatings was left in as-sprayed and as-received states, respectively. The surface roughness was smoothened during the first abrasive cycle and was not included in the wear rate calculation.

The sliding-wear resistance and coefficient of friction (COF) were evaluated using the ball-on-flat test, according to ASTM G133. Test parameters were as follows: 25 N load; steel 100Cr6, 6-mm-diameter ball counterpart; 5 Hz oscillating frequency; 10 mm stroke length; and 1000 s testing time. For each coating, three different measurements were performed. The wear tracks' profiles were measured by the profilometer KLA-Tencor P-6 Profiler, at three different places, and the wear volume was calculated. Prior to sliding-wear tests, the surface of the coating was ground and polished to the 0.04 ± 0.02 Ra value.

Both abrasive and adhesive wear was characterized by the coefficient of wear K [mm^3/Nm], calculated from the coating volume loss, used load and the abrasive or sliding distance:

$$K = \frac{V}{L.s}, \tag{Eq 1}$$

where V is the volume loss (mm^3), L (N) is the load, and s (m) is the abrasive or sliding distance.

After the tests, the SEM of the wear tracks was observed, to indentify the wear mechanism.

3. Results and Discussion

3.1 Microstructure

The microstructure of HVOF as-sprayed coatings and annealed coatings can be seen and compared in Fig. 1(a-d). The coatings' microstructure consists of individual splats. In the splats, the dendritic structure of Co-based material can be recognized. No hard precipitates were identified, either for feedstock, as-sprayed or annealed coating. On the intersplat boundaries, the minor oxidation is concentrated, as well as a thin layer of oxides, originated from oxidation during the spraying process. No significant changes of the coatings' microstructure as a result of annealing were found by SEM or BSE observation.

The analyses of phase composition (Fig. 2) revealed that feedstock powder contains only an fcc Co-based solid solution (the refined lattice parameter is 3.5813 ± 0.0004 Å, which means that the elemental lattice is larger than for pure α-Co of 3.5442 Å (Ref 49)) and no reflections corresponding to hcp Co or precipitated carbides were detected. However, on the as-sprayed surface, both fcc and hcp Co are present, and based on Rietveld analysis, more than 30% of the irradiated volume changed its structure from fcc to hcp Co-based solid solution. As shown in Fig. 2, the reflections are broadened, which correspond to fine crystallites, or small sizes of coherently scattering domains, in the region of lower tens of nanometers. The lattice parameter of α-Co is further increased as compared to feedstock, to around 3.60 Å, indicating a more pronounced shift from pure Co, and the lattice parameters of hexagonal Co have a c/a ratio of about 1.51, which is significantly less than 1.62 for the pure phase. No carbide precipitation or oxidation is seen in the as-sprayed Stellite 6 coatings. In former studies (Ref 14, 34, 44), the absence of carbides and oxides in the HVOF-sprayed Stellite 6 was confirmed, but no hcp Co-based phase was reported up to now. In both studies (Ref 14, 44), a small amount of M_7C_3 carbide was recorded in the feedstock powder. That feedstock was different than the feedstock used in our case (Jet-Kote 7206 in the Sidhu's study and unlabeled powder in Zhang's study). In as-sprayed coating, a very small peak of M_7C_3 carbide was identified by XRD, but not confirmed using SEM in the work of Zhang, and no carbide was found in the work of Sidhu. The authors of both studies deduced that the precipitation of carbides was suppressed by the high rate of cooling.

A possible explanation for the differences in microstructure phase composition can be in higher heat input during spraying in comparison with reported coatings. For spraying, different technological parameters can be used, leading to different levels of microstructure changes. The influence of spraying parameters on phase composition was intensively studied for hardmetal coatings (Ref 50, 51), concerning namely the dissolution of
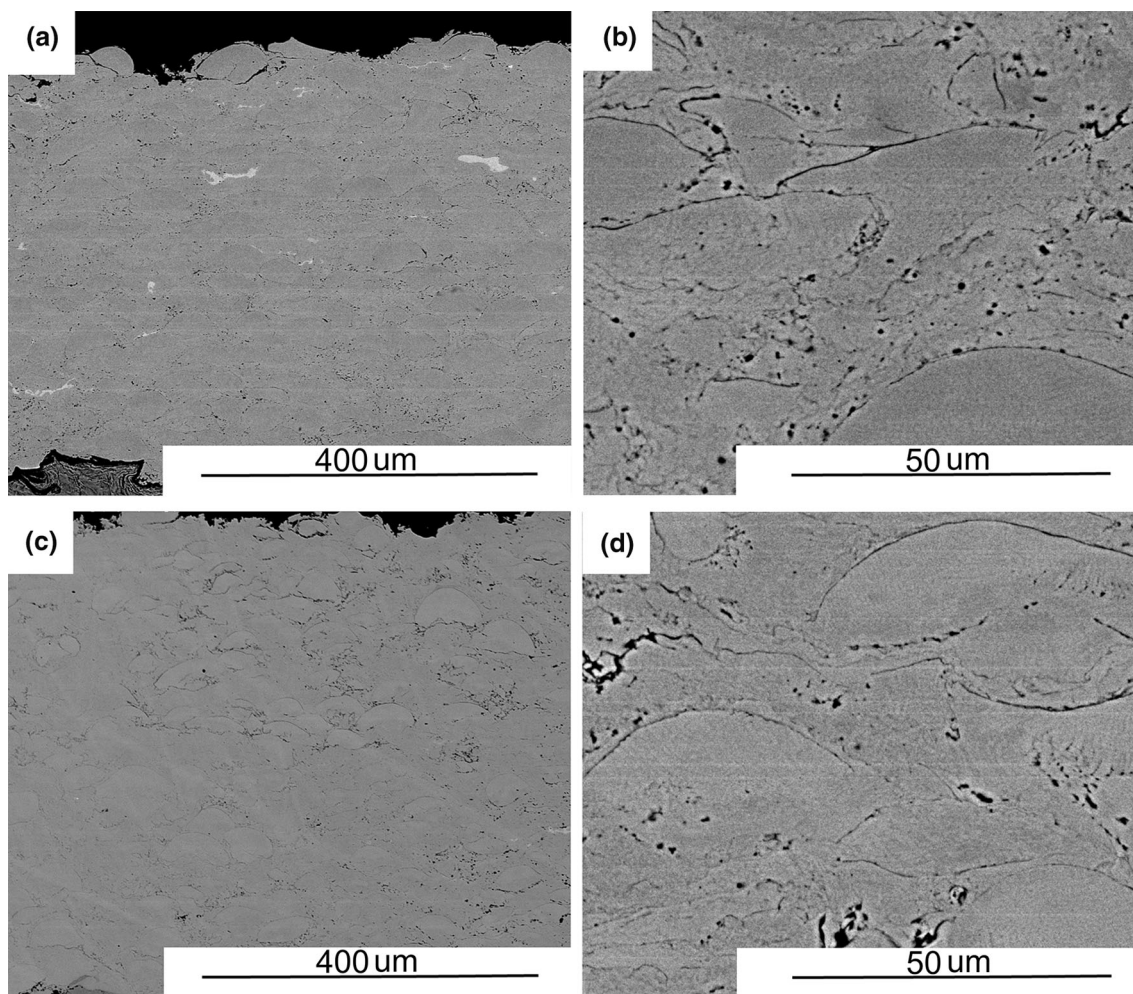
Fig. 1 BSE micrographs of HVOF as-sprayed (a, b) and 600 °C/116 h annealed (c, d) Stellite 6 coatings microstructures
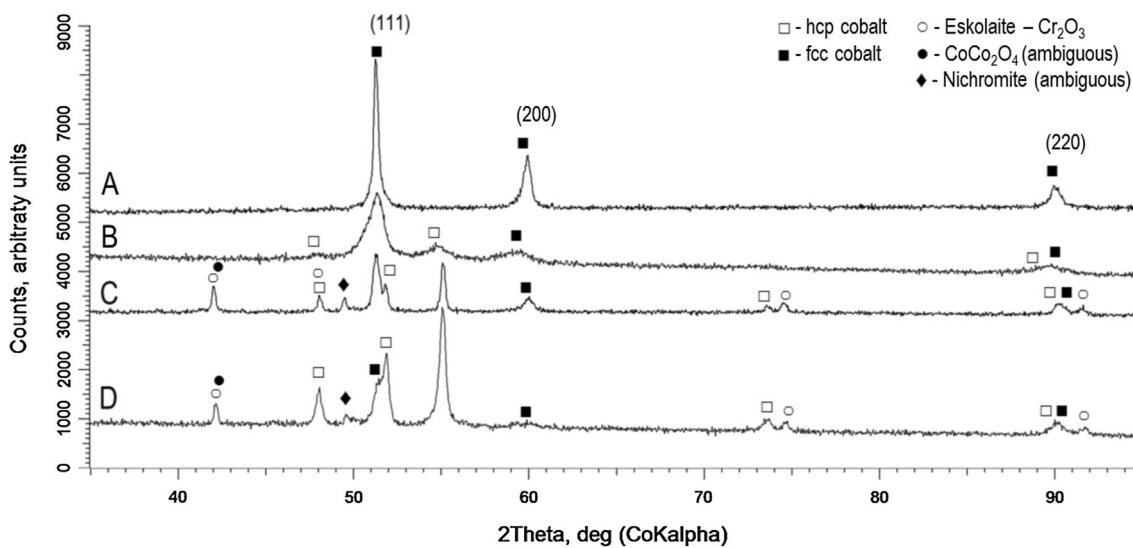

Fig. 2 Measured powder XRD patterns for feedstock powder (*A*), surface of the as-sprayed coating (*B*), surface of the as-received (*C*) and ground (*D*) annealed coating

Table 2 Phase content of evaluated materials based on the Rietveld analysis

Phase composition (%)	Co-fcc	Co-hcp	Cr_2O_3	$NiCr_2O_4$	$CoCo_2O_4$
Powder feedstock	100	...	...	...	...
As-sprayed coating	70	30	...	...	
Annealed 600 °C/116 h	47	41	9	2.5	0.5
Annealed 600 °C/116 h ground	16	82	0.6	0.3	0.5
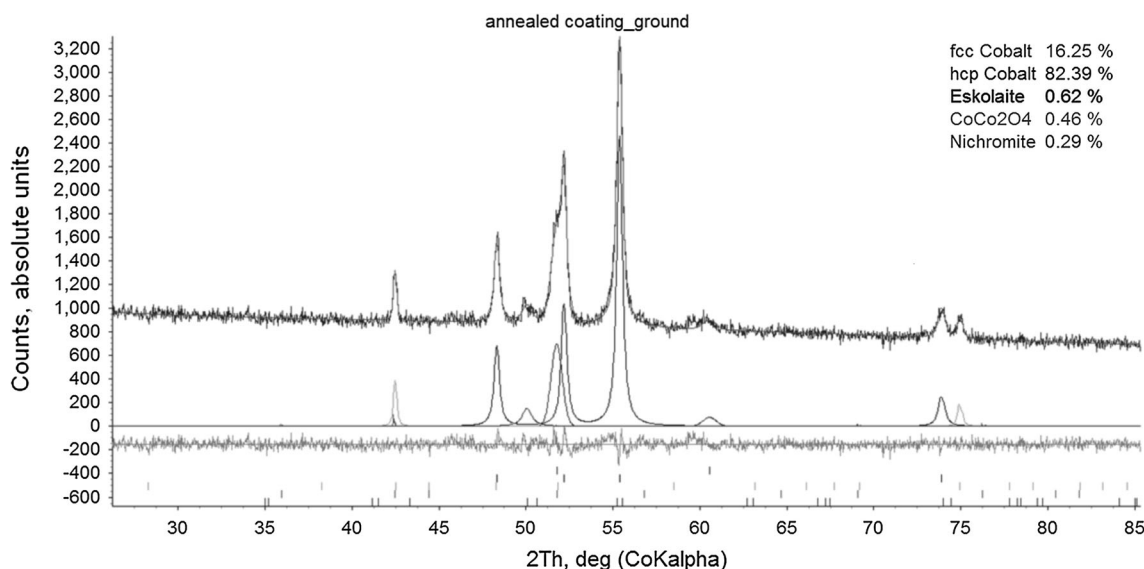
Fig. 3 Result of Rietveld refinement of XRD pattern measured on annealed coating after grinding

carbides into the matrix and related degradation of coating properties. No study concentrating on the phase composition of Co-based coatings relating to the spraying parameters has been found. The optimization procedures are focused mainly on the level of porosity or oxidation on the splat boundaries (Ref 52). The lack of carbides can be explained by the absence of strong carbide formers such as Nb, Ta or Zr in the feedstock powder.

The annealing in an air atmosphere at 600 °C for 116 h further increased the hcp-phase amount in the coatings' structure. The measurement of the oxidized surface indicated more than 40 wt.% of hcp phase according to Rietveld analysis. Together with the fcc and hcp Co-based solid solution, the expected occurrence of oxides was recorded. The formation of the major Cr_2O_3 oxide and minor $NiCr_2O_4$ and $CoCo_2O_4$ spinel oxides during exposure to high temperatures was described previously by Sidhu and Kong (Ref 35, 39). While the presence of eskolaite (Cr_2O_3) is evident from the phase identification of the XRD pattern, the assigning of the nichromite and $CoCo_2O_4$ phases is ambiguous due to low intensity and significant overlap of the reflections.

After removing the oxide layer on the surface, the oxide content decreased significantly (see Table 2 and the Rietveld refinement in Fig. 3). Even more hcp phase was measured on the ground surface of annealed Stellite 6 samples. The significant increase (82 versus 41 wt.% of hcp in the as-received annealed sample) is partly influ-

enced by the reduction in oxides, but the main reason has to be elsewhere. A possible explanation can be found in the stress-induced fcc to hcp martensitic transformation, taking place during metallographic grinding and polishing. Lattice parameters refined from XRD patterns are 3.5609 ± 0.006 Å (an as-received) and 3.547 ± 0.001 Å (ground) for α-Co, and the c/a ratio for hcp is 1.6145 and 1.6120 for as-received and ground annealed surfaces, respectively. To precisely quantify the amount of the hcp phase transformed during heat treatment, annealing in an inert atmosphere should be done in the future to exclude the influence of oxidation. Furthermore, a more sophisticated technique of sample preparation should be used to avoid the possible stress-induced martensitic transformation.

3.2 Microhardness

The microhardness HV0.3 measured on the ground surface was higher for annealed coating (740 ± 50) than for as-sprayed coating (635 ± 75). The thermal spray anisotropy is responsible for the difference in the in-plane and cross section microhardness value, but a similar tendency can be observed for the microhardness depth profile (see Fig. 4). The microhardness of annealed coating is slightly higher across the whole thickness, even though the scatter is high due to the inhomogeneity of thermally sprayed coatings. For Cr-Cr-Mo alloys, the hcp structure
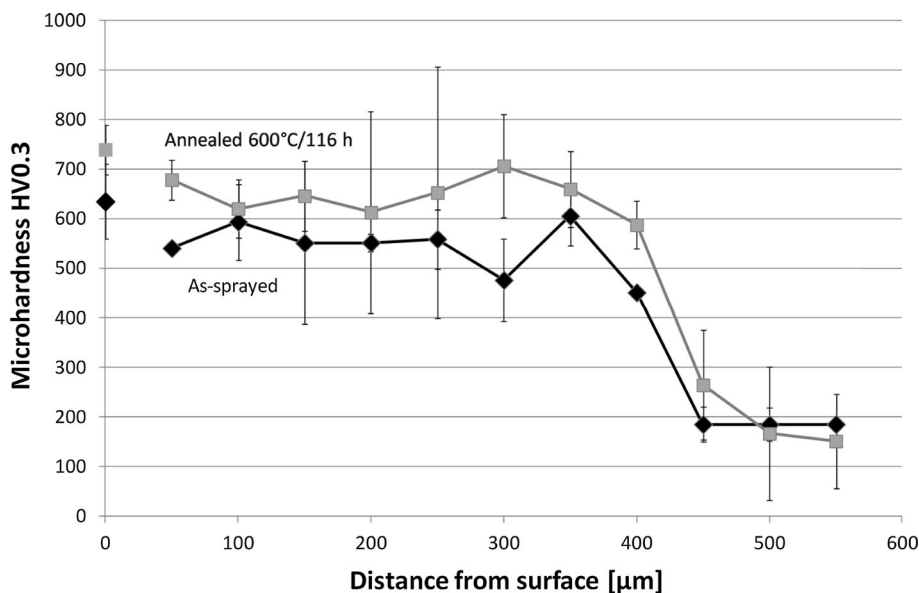
Fig. 4 Microhardness depth profile of as-sprayed and annealed coating

was reported to be harder and less ductile compared to fcc (Ref 10, 11). The amount of the hcp phase in annealed coating can contribute to the increase in hardness.

3.3 Cohesion

The high-load (150 N) Vickers indents were smaller when the annealed coating was measured (212 ± 4 μm versus 230 ± 7 μm), which is in agreement with the microhardness measurement in Fig. 4.

Also, the length of the cracks, originated near the Vickers corners, was much shorter in the case of annealed coatings. The average crack length of as-sprayed coating reached 152 ± 30 μm, while the average crack length of annealed coating was only 95 ± 35 μm. This implies that the cohesion of annealed coating is higher compared to as-sprayed coating. The microscopic observation showed that the main reason for such a finding can be connected with hardness. The cracks spread exclusively along the inter-splat boundaries (Fig. 5), regardless of the coating state. With as-sprayed coating, the indentation was accompanied by a bigger deformation of indents surrounding, leading to the creation of numbers of decohesions between the individual splats. The deformation contributes to the main crack opening and further increase in the length of the crack.

The higher strength of annealed coating is responsible not only for greater hardness, but also for lower deformation and consequently for shorter and less branched cracks. The observed mechanism of cracks spreading differs from the mechanisms described previously for brittle hardmetal and ceramic thermally sprayed coatings (Ref 53, 54). The indentation fracture toughness models, developed for brittle materials (Ref 48), presumed the creation of one main crack, originated from the Vickers

indents corner. They are not valid for Co-based alloy HVOF-sprayed coatings; thus, the value of indentation fracture toughness cannot be calculated in this case.

However, the observation of lower intersplat cohesion, connected with higher local deformation, is in agreement with the wear mechanism of as-sprayed coating reported below.

3.4 Abrasive Wear Resistance

The abrasive wear resistance, determined according to ASTM G-65, showed that the as-sprayed Stellite 6 coating is worn out slower than annealed coating (Fig. 6). During the first cycle (148 m of abrasive distance), the material volume loss was higher in the case of as-sprayed coating, but after that the wear rate was lower. The same results, expressed by Wear Coefficient K (mm^3/Nm), are shown in Fig. 7 and in Table 3.

The SEM of worn surfaces can be compared in Fig. 8. A similar wear mechanism was identified for both as-sprayed and annealed coatings—abrasive wear. The grooves remaining after the abrasive Al_2O_3 particles are present in both samples; no splat delamination was observed. Nevertheless, the surface of annealed coating seems to be smoother, with the grooves and scratches oriented in the same way. This would correspond with slightly higher hardness and lower ductility of annealed coating with a content of the hcp phase.

The contradiction of higher hardness and lower wear resistance was already observed and reported in a comparative study (Ref 55). It was shown that in the group of alloy-based HVOF coatings, higher hardness is not necessarily an indicator of higher wear resistance. The harder NiCrBSi HVOF coating showed lower wear resistance than softer, but more ductile, high-chrome steel coating.
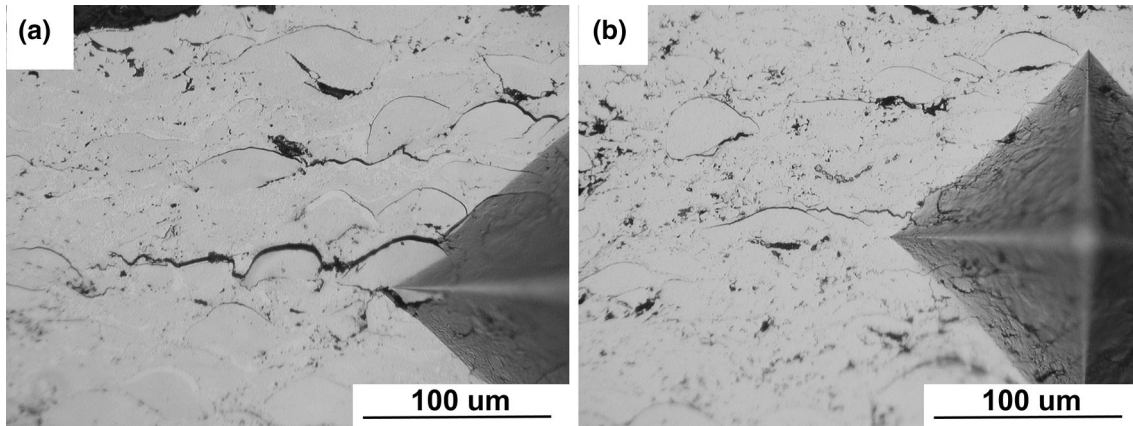
Fig. 5 Cracks originated from the corner of Vickers indents in (a) as-sprayed; (b) annealed coating
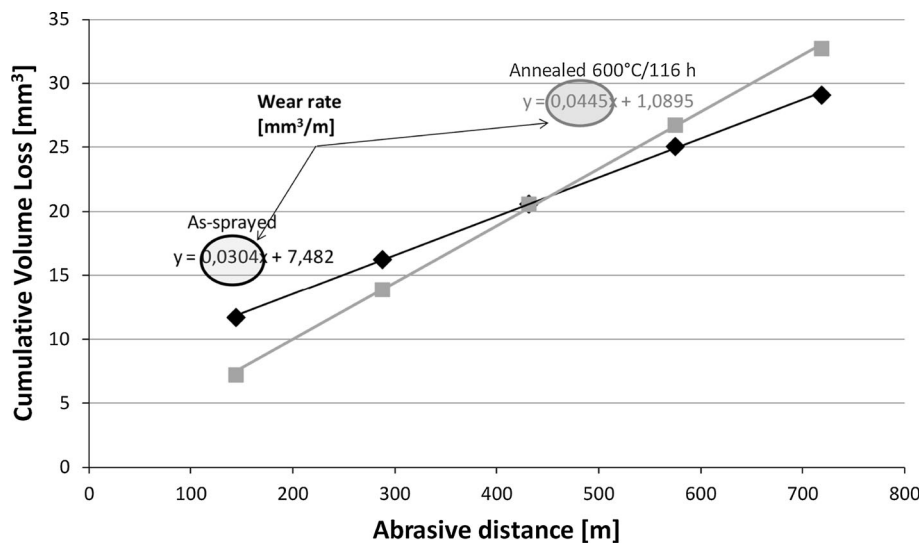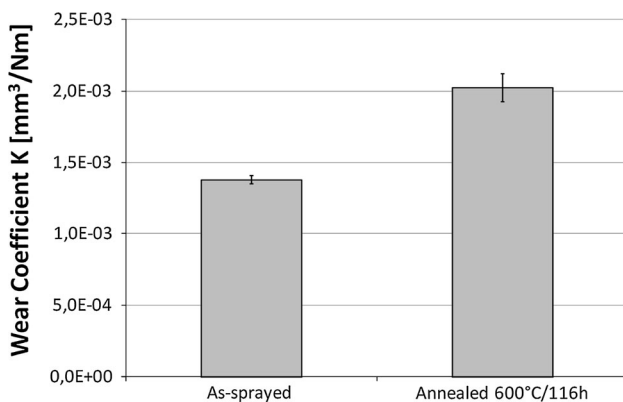

Fig. 6 Abrasive wear rate

Fig. 7 Abrasive wear coefficient of as-sprayed and annealed coatings

Table 3 Wear coefficient of as-sprayed and annealed coating

Wear coefficient K (mm^3/Nm)	ASTM G-65	ASTM G-133
As-sprayed coating	$(1.39 \pm 0.03) \times 10^{-3}$	$(4.31 \pm 0.64) \times 10^{-5}$
Annealed 600 °C/116 h	$(2.02 \pm 0.09) \times 10^{-3}$	$(5.60 \pm 0.95) \times 10^{-5}$

(Ref 56). The wear grooves in a worn steel surface were short and oriented in various directions, similar to the as-sprayed Stellite 6 coating. This is indicative of the influence of the embedded Al_2O_3 particles. The mechanism of increasing the wear resistance by progressive embedding of hard abrasive particles in the coating surface during the wear test in the case of metallic coatings is described in the literature (Ref 57, 58).

Comparing the dry sand rubber-wheel test results of Fe and Ni-based HVOF-sprayed coatings (Ref 59), the Stellite 6 has lower wear resistance (1.39×10^{-3} versus

The heavy plastic deformation of the steel coating was not accompanied by higher material loss, compared to the coating with higher hardness, more prone to microcutting
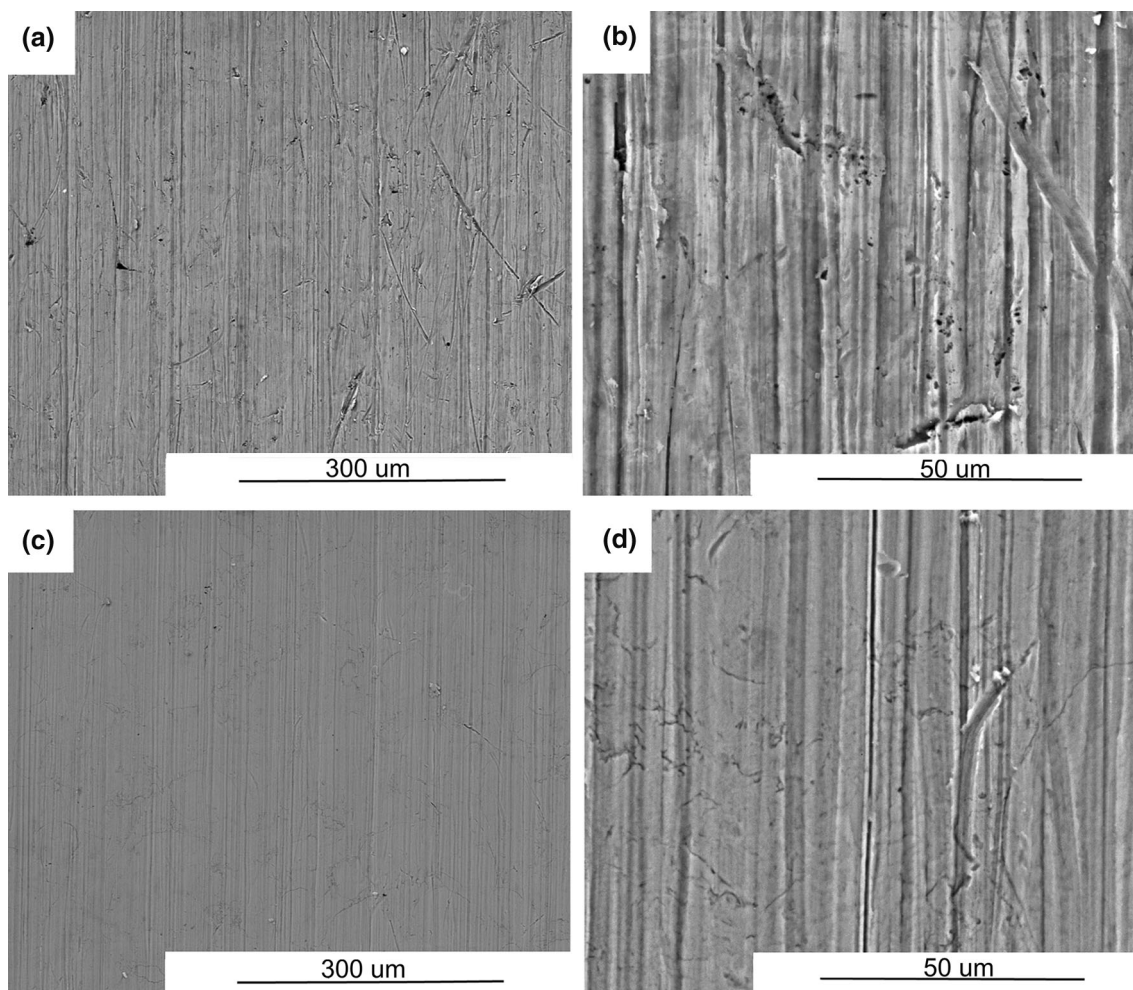
Fig. 8 SEM of worn surface after abrasion wear tests of HVOF as-sprayed (a, b) and 600 °C/116 h annealed (c, d) Stellite 6 coatings microstructures

0.7×10^{-3} and 1.1×10^{-3} for Fe-Ni-Cr-B-C and Fe-Ni-Cr-Mo-B-C coating, respectively). However, in that study, SiO_2 abrasive medium was used, while the present study used Al_2O_3-based medium, and this difference in the experimental conditions has to be taken into consideration. Specifically, the type of abrasive particles plays a significant role, as shown in (Ref 60). The sharp-edged corundum grains used for Stellite 6 coating testing can be more aggressive than less hard SiO_2.

3.5 Adhesive Wear Resistance

The adhesive wear resistance of Stellite 6 coating, determined according to ASTM G-133, is also better in the as-sprayed state than after heat exposure (Fig. 9). The sliding behavior is illustrated in Fig. 10, where the coefficient of friction evolution is recorded. The first period, characterized by low friction between the coating and the chrome steel counterpart, is similar for both as-sprayed and annealed coating. After that, a sudden increase also appeared for both coatings. The new steady COF value of as-sprayed coating varied between 0.5 and 0.6, which is in

line with common COF values (Ref 3), and has a high level of fluctuation. The annealed coatings' COF, on the contrary, exhibited a very stable and smooth evolution, with the lower value of around 0.45. The length of the first period differs for each measurement. The COF evolution has to be correlated with wear-track observation and wear-mechanism evaluation (Fig. 11).

The HVOF alloy coatings wear mechanisms under the sliding load were described in great detail in the work of Bolelli et al. (Ref 59, 61-63). Three main mechanisms can be identified during sliding: (1) abrasive wear (2) adhesive wear and (3) brittle delamination. The abrasive wear takes place when one of the mating materials is significantly softer than the other. Such wear is observed typically during the wear tests using an Al_2O_3 counterpart, or if hard particles such as carbides or oxides are present in the wear track (Ref 59). The adhesive wear mechanism consists of the creation of microwelds between the asperities of the surfaces. The continuous movement of the two main bodies leads to the rupture of the microweld and usually a small part of the material with lower strength. Such behavior is more prone to appear if the mating materials are chemically
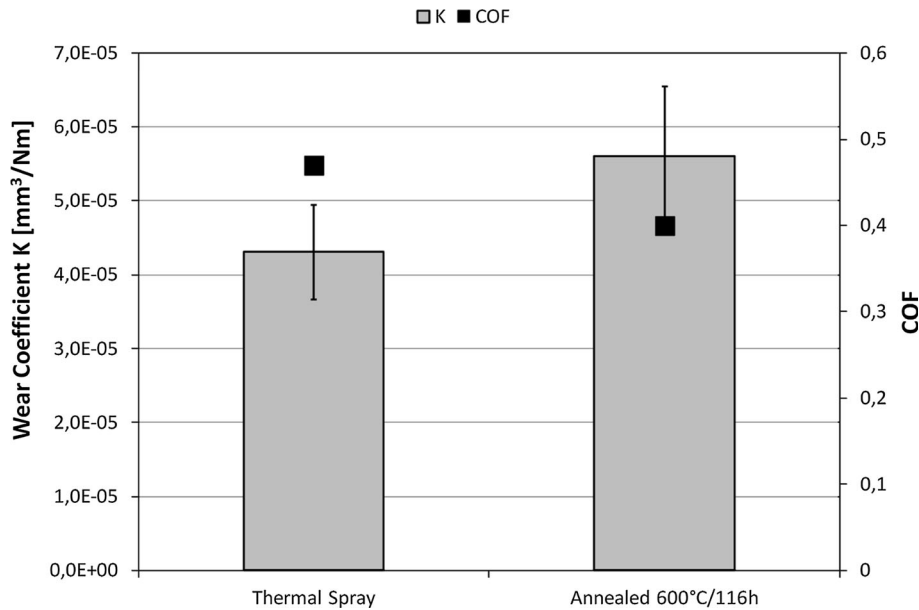
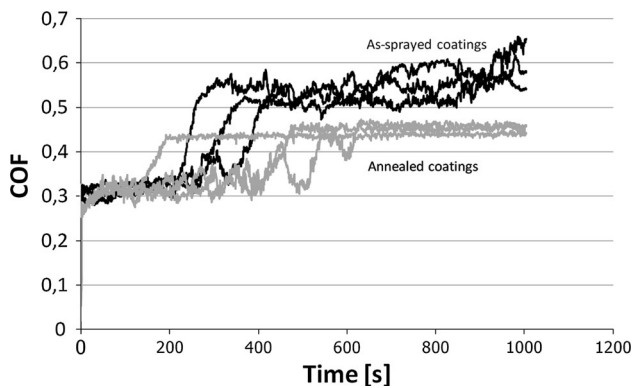**Fig. 9** Adhesive wear coefficient of as-sprayed and annealed coatings

Fig. 10 COF evolution of as-sprayed and annealed coatings during linearly reciprocation wear test according to ASTM G-133

close—such as in the case of a 100Cr steel counterpart in the sliding tests. The pulled-out material is further deformed and heated up by continuous movement. It can stick to the surface of both coating and counterpart. The high temperature leads to oxidation of the wear debris, which can later create an oxide tribofilm with a possibly positive effect on the following wear process. If the material is less ductile, the repeated loading and deformation can lead to the creation of subsurface fatigue cracks, leading to delamination. The thermally sprayed coatings with their lamellae structure are sensitive to Hertzian loading. The alloy coatings, containing oxides on the intersplat boundaries, are even more prone to delamination. Similarly to the adhesive wear mechanism, the wear debris is deformed and oxidized. Some of it can be

found in the delaminated areas, and some can create a continuous tribofilm.

In Fig. 11, the wear tracks of as-sprayed and annealed Stellite 6 coating can be compared. The two main features can be recognized in the wear tracks—delamination of the splats and the areas of deformed material, from either the coating or the counterpart. Delamination of the whole particles is responsible for higher and fluctuating COF, namely in the case of the as-sprayed coating (Fig. 11a, b). The mechanism observed during the cohesion strength evaluation can contribute to the creation and further spreading of intersplat cracks and delamination. The deformed oxidized wear debris material is also visible on the surface of the as-sprayed coating, but in a smaller amount compared to annealed coating. The wear track of the annealed coating contains the signs of plowing or abrasive grooves, as well as more evenly spread tribofilm (Fig. 11c). However, the delamination mechanism was also part of the wear process (Fig. 11d).

The more uniform tribofilm, and less pronounced delamination, is probably responsible for lower and more stable COF. Nevertheless, the wear rate of the harder annealed coating is higher compared to the as-sprayed coating. In order to explain the discrepancy, the possible fcc to hcp strain-induced transformation can be suggested. During the wear process, the martensitic transformation can be under progress, increasing the wear resistance of as-sprayed coating to a greater extent than that of annealed coating, similarly to Co-Cr-Mo alloys (Ref 5-10). To confirm the suggestion, the XRD measurement in the wear track should be done and compared in subsequent research.
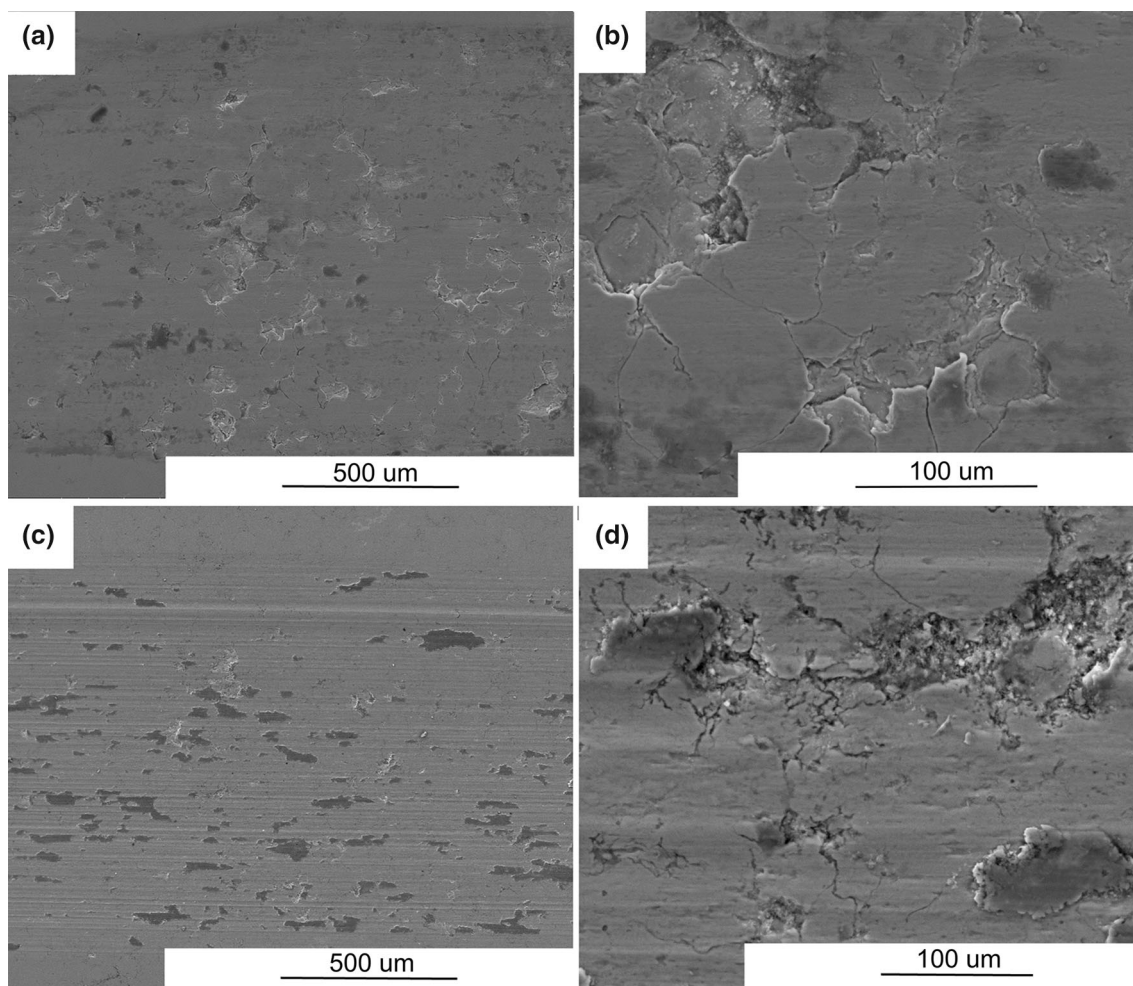
Fig. 11 SEM of worn surface after sliding-wear tests of HVOF as-sprayed (a, b) and 600 °C/116 h annealed (c, d) Stellite 6 coatings microstructures

4. Conclusion

The influence of heat treatment on the microstructure and tribological behavior of Co-Cr-W Stellite 6 alloy HVOF-sprayed coating was analyzed. It was found that while the feedstock material is composed of Co-based solid solution in the fcc structure, the as-sprayed coating contains around 30 wt.% of the hcp phase. The process of transformation from metastable fcc to stable hcp is caused by heating during spraying. The transformation further continued during thermal post-treatment and during surface finishing. The heat treatment in an air atmosphere led to the creation of an oxide layer on the coating surface, consisting of major Cr_2O_3 and minor spinel oxides. The same oxides, but in a minor amount, were found also inside the heat-treated coating. No hard precipitates appeared in the coating as a result of spraying or heat treatment.

In relation to phase changes, a small increase in hardness and cohesive strength was found, which resulted in differences in the wear mechanisms of both abrasion and sliding. Greater hardness and a lower tendency to inter-splat delamination led to a smoother surface of the wear tracks and a lower coefficient of friction. However, the measured wear resistance of annealed coating was lower, in contradiction to better mechanical properties. To explain the discrepancy, the possible strain-induced martensitic fcc to hcp transformation during wear loading can be suggested, but has to be confirmed in further studies.

References

1. http://www.stellite.com/AboutKennametalStellite/KennametalStelliteDatasheets/tabid/339/Default.aspx.

2. T. Ericsson, The temperature and concentration dependence of the stacking fault energy in the Co-Ni system, *Acta Metall.*, 1966, **14**(7), p 853-865

3. W. Betteridge, *Cobalt and Its Alloys*, Ellis Horwood, Chichester, 1982

4. Q. Meng, S. Guo, X. Zhao, and S. Veintemillas-Verdaguer, Bulk metastable cobalt in fcc crystal structure, *J. Alloy Compd.*, 2013, **580**, p 187-190

5. X. Wu, N. Tao, Y. Hong, J. Lu, and K. Lu, γ-ε Martensite transformation and twinning deformation in fcc cobalt during surface mechanical treatment, *Scr. Mater.*, 2005, **52**, p 547-551

6. M.L. Benson, B. Reez, P.K. Liaw, W. Riemers, H. Choo, D.W. Brown, T.A. Saleh, and D.L. Klastrom, Phase-transformation and subgrain-deformation characteristics in cobalt-based superalloy, *Mater. Sci. Eng. A*, 2011, **258**, p 1987-1993

7. M.L. Benson, P.K. Liaw, H. Choo, D.W. Brown, M.R. Daymond, and D. Klastrom, Strain-induced phase transformation in cobalt-based superalloy during different loading modes, *Mater. Sci. Eng. A*, 2011, **528**, p 6051-6058

8. H. Matsumoto, Y. Koizumi, T. Ohashi, B.-S. Lee, Y. Li, and A. Chiba, Microscopic mechanism of plastic deformation in polycrystalline Co-Cr-Mo alloy with a single hcp phase, *Acta Mater.*, 2014, **64**, p 1-11

9. K. Yamanaka, M. Mori, Y. Koizumi, and A. Chiba, Local strain evolution due to the athermal γ-ε martensitic transformation in biomedical Co-Cr-Mo alloys, *J. Mech. Behav. Biomed. Mater.*, 2014, **32**, p 52-61

10. A. Chiba, K. Kumagai, N. Nomura, and S. Miyakawa, Pin-on-disk wear behaviour in like-on-like configuration in a biological environment of high carbon cast and low carbon forget Co-29Cr-6Mo alloys, *Acta Mater.*, 2007, **55**, p 1309-1318

11. Y. Chen, Y. Li, S. Kurosu, K. Yamanaka, N. Tang, Y. Koizuni, and A. Chiba, Effect of sigma phase and carbide on the wear behaviour of Co-Cr-Mo alloys in Hanks solution, *Wear*, 2014, **310**, p 51-62

12. C. Balagna, S. Spriano, and M.G. Faga, Characterization of Co-Cr-Mo alloys after a thermal treatment for high wear resistance, *Mater. Sci. Eng. C*, 2012, **32**, p 1868-1877

13. M. Mori, K. Yamanaka, and A. Chiba, Phase decomposition in biomedical Co-29Cr-6Mo-0.2N during isothermal heat treatment at 1073K, *J. Alloy. Compd.*, 2014, **590**, p 411-416

14. T.S. Sidhu, S. Prakash, and R.D. Agrawal, Studies of the metallurgical and mechanical properties of high velocity oxy-fuel sprayed stellite-6 coatings on Ni- and Fe-based superalloys, *Surf. Coat. Technol.*, 2006, **201**, p 273-281

15. A.F. Farnia, J.C. Malek Ghaini, V. Rao, J.Th. Ocelík, and M. De Honson, Effect of Ta on the microstructure and hardness of Stellite 6 coating deposited by low power pulse laser treatments, *Surf. Coat. Technol.*, 2012, **213**, p 278-284

16. A. Frenk and W. Kurz, Microstructural effects on the sliding wear resistance of a cobalt-based alloy, *Wear*, 1994, **174**, p 81-91

17. R. Ahmed, A. Ashraf, M. Elameen, N.H. Faisal, A.M. El-Sherik, Y.O. Elakwah, and M.F.A. Goosen, Single asperity nanoscratch behaviour of HIPed and cast stellite 6 alloys, *Wear*, 2014, **312**, p 70-82

18. S. Apay and B. Gulec, Wear properties of AISI, 1015 steel coated with stellite 6 by microlaser welding, *Mater. Des.*, 2014, **5**, p 1-8

19. A. Frenk, M. Vandyoussefi, J.-D. Wagnière, A. Zryd, and W. Kurz, Analyses of the laser-cladding process for stellite on steel, *Metall. Mater. Trans. B*, 1997, **28B**, p 501-508

20. A.S.C.M. d'Oliveira, R. Vilar, and C.G. Feder, High temperature behavior of plasma transferred arc and laser Co-based coatings, *Appl. Surf. Sci.*, 2001, **201**, p 154-160

21. A.S.C.M. d'Oliveira, P.S.C.P. da Silva, and R. Vilar, Microstructural features of consecutive layers of Stellite 6 deposited by laser cladding, *Surf. Coat. Technol.*, 2002, **153**, p 203-209

22. U. de Oliveira, V. Ocelík, and J.Th.M. de Hosson, Residual stress analyses in Co-based laser clad layers by laboratory X-ray and synchrotron diffraction techniques, *Surf. Coat. Technol.*, 2006, **201**, p 533-542

23. U. de Oliveira, V. Ocelík, and J.Th.M. de Hosson, Microstresses and microstructure in thick cobalt-based laser deposited coatings, *Surf. Coat. Technol.*, 2007, **201**, p 6363-6371

24. V. Ocelík, U. de Oliveira, and J.Th.M. de Hosson, Thick Co-based coating on cast iron by side laser cladding: analysis of processing conditions and coating properties, *Surf. Coat. Technol.*, 2007, **201**, p 5875-5883

25. V. Ocelík, J. Bosgra, and J.Th.M. de Hosson, In-situ strain observation in high power laser cladding, *Surf. Coat. Technol.*, 2009, **203**, p 3189-3196

26. V. Ocelík, I. Furár, and J.Th.M. De Hosson, Microstructure and properties of laser clad coatings studied by orientation imaging microscopy, *Acta Mater.*, 2010, **58**, p 6763-6772

27. V. Ocelík, M. Eekma, I. Hemmati, and J.Th.M. De Hosson, Elimination of start/stop defects in laser cladding, *Surf. Coat. Technol.*, 2012, **206**, p 2403-2409

28. R. Jendrzejewski, A. Conde, J.J. de Damborenea, and G. Śliwiński, Characterisation of the laser-clad satellite layers for protective coatings, *Mater. Des.*, 2002, **23**, p 83-88

29. R. Jendrzejewski and G. Śliwiński, Investigation of temperature and stress fields in laser cladded coatings, *Appl. Surf. Sci.*, 2007, **254**(4), p 921-925

30. R. Jendrzejewski, C. Navas, A. Conde, J.J. de Damborenea, and G. Śliwiński, Properties of laser-cladded satellite coatings prepared on pre-heated chromium steel, *Mater. Des.*, 2008, **29**, p 187-192

31. A. Gholipour, M. Shamanian, and F. Ashrafizadeh, Mirostructure and wear behavior of stellite 6 cladding on 17-4 PH stainless steel, *J. Alloy. Compd.*, 2011, **509**, p 4905-4909

32. R. Singh, D. Kumar, S.K. Mishra, and S.K. Tiwari, Laser cladding of Stellite 6 on stainless steel to enhance solid particle erosion and cavitation resistance, *Surf. Coat. Technol.*, 2014, **251**, p 87-97

33. A. Kusmoko, D. Dunne, H. Li, and D. Nolan, Effect of two different energy inputs for laser cladding of stellite 6 on P91 and P22 steel substrates, *Proc. Mater. Sci.*, 2014, **6**, p 26-36

34. T.S. Sidhu, S. Prakash, and R.D. Agrawal, Hot corrosion resistance of high-velocity oxyfuel sprayed coatings on a nickel-base superalloy in molten salt environment, *J. Therm. Spray Technol.*, 2006, **15**(3), p 387-399

35. T.S. Sidhu, S. Prakash, and R.D. Agrawal, Hot corrosion studies of HVOF NiCrBSi and Stellite-6 coatings on a Ni-based superalloy in an actual industrial environment of coal fired boiler, *Surf. Coat. Technol.*, 2006, **201**, p 1602-1612

36. B.S. Sidhu and S. Prakash, Performance of NiCrAlY, Ni-Cr, Stellite-6 and Ni3Al coatings in Na2SO4-60%V2O5 environment at 900°C under cyclic conditions, *Surf. Coat. Technol.*, 2006, **201**, p 1643-1654

37. H.S. Sidhu, B.S. Sidhu, and S. Prakash, Solid particle erosion of HVOF sprayed NiCr and Stellite-6 coatings, *Surf. Coat. Technol.*, 2007, **202**, p 232-238

38. T.S. Sidhu, S. Prakash, and R.D. Agrawal, A comparative study of hot corrosion resistance of HVOF sprayed NiCrBSi and Stellite-6 coated Ni-based superalloy at 900 °C, *Mater. Sci. Eng. A*, 2007, **445-446**, p 210-218

39. N. Jegadeeswaran, K.U. Bhat, and M.R. Ramesh, Oxidation studies on as-received HVOF sprayed Stellite 6 coating on turbine alloys at 800 °C, *Int. J. Curr. Eng. Technol.*, 2013, **4**(6), p 214-220

40. L. Moskowitz and K. Trelewicz, HVOF coatings for heavy-wear, high-impact applications, *J. Therm. Spray Technol.*, 1997, **6**(3), p 294-299

41. P.V. Marques and C.R.C. Lima, Studies of cavitation resistant thermally sprayed and welded coatings, *Thermal Spray 2003: Advancing the Science and Applying the Technology*, C. Moreau and B. Marple, Ed., ASM International, Materials Park, OH, 2003, p 389-393

42. A. Kumar, J. Boy, R. Zatorski, and L.D. Stephenson, Thermal spray and weld repair alloys for repair of cavitation damage in turbines and pumps: a technical note, *J. Therm. Spray Technol.*, 2005, **14**(2), p 177-182
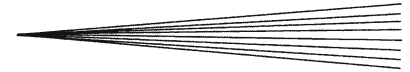
43. A. Kusmoko, D. Dunne, and H.A. Li, A comparative study for wear resistant of Stellite 6 on Nickel alloy substrate produced by laser cladding, *HVOF and plasma spraying techniques, International Journal of Current Engineering and Technology*, 2014, **4**(1), p 32-36

44. D. Zhang, S.J. Harris, and D.G. McCartney, Mechanical properties and microstructure of HVOF sprayed Co and Ni alloy coatings, *Proceeding of ITSC 2013 Thermal Spray 2003: Advancing the Science and Applying the Technology*, B.R. Marple and C. Moreau, Ed., ASM International, Materials Park, OH, 2003, p 829-836

45. Š. Houdková, J. Černý, Z. Pala, and P. Haušild, High Temperature Resistance of Selected HVOF Coatings, *Key Eng. Mater.*, 2015, **662**, p 111-114

46. H.M. Rietveld, A profile refinement method for nuclear and magnetic structures, *J. Appl. Crystallogr.*, 1969, **2**(2), p 65-71

47. R.W. Cheary and A. Coelho, A fundamental parameters approach to X-ray line-profile fitting, *J. Appl. Crystallogr.*, 1992, **25**(2), p 109-121

48. C.B. Ponton and R.D. Rawlings, Vickers indentation fracture toughness test Part 1 Review of literature and formulation of standardized indentation toughness equations, *Materials Science Technology*, 1989, **5**, p 865-872

49. A. Taylor and R.W. Floyd, Precision measurements of lattice parameters of non-cubic crystals, *Acta Crystallogr. A*, 1950, **3**(4), p 285-289

50. R. Schwetzke and H. Kreye, Microstructure and properties of tungsten carbide coatings sprayed with various high velocity oxygen fuel spray system, *J. Therm. Spray Technol.*, 1999, **8**, p 433-439

51. L.-M. Berger, S. Saaro, T. Naumann, M. Kašparová, and F. Zahálka, Influence of feedstock powder characteristics and spray processes on microstructure and properties of WC-(W, Cr) 2C-Ni hardmetal coatings, *Surf. Coat. Technol.*, 2010, **205**(4), p 1080-1087

52. Š. Houdková, M. Kašparová, and J. Schubert, The spraying parameters optimization of the HVOF Stellite 6 coating. in *METAL 2012: 21nd International Conference on Metallurgy and Materials.* (Ostrava: TANGER, 2012), p 947-953

53. D. Chicot, G. Duarte, A. Tricoteaux, B. Jorgowski, A. Leriche, and J. Lasage, Vickers indentation fracture (VIF) modeling to analyze multi-cracking toughness of titania, alumina and zirconia plasma sprayed coatings, *Mater. Sci. Eng. A*, 2009, **527**, p 65-76

54. N.H. Faisal, J.A. Steel, R. Ahmed, and R.L. Reuben, The use of acoustic emission to characterize fracture behavior during Vickers indentation of HVOF thermally sprayed WC-Co coatings, *J. Therm. Spray Technol.*, 2009, **18**(4), p 525-535

55. Š. Houdková, F. Zahálka, M. Kašparová, and L.-M. Berger, Comparative study of thermally sprayed coatings under different types of wear conditions for hard chromium replacement, *Tribol. Lett.*, 2011, **42**(2), p 139-154

56. B. Bhushnan, *Principles and Applications of Tribology*, Wiley, New York, 1999, p 479-585

57. G. Bolelli, V. Cannillo, L. Lusvarghi, and T. Manfredini, Wear behavior of thermally sprayed ceramic oxide coatings, *Wear*, 2006, **261**, p 1298-1315

58. G. Bolelli, V. Cannillo, L. Lusvarghi, and S. Riccò, Mechanical and tribological properties of electrolytic hard chrome and HVOF-sprayed coatings, *Surf. Coat. Technol.*, 2006, **200**, p 2995-3009

59. A. Milanti, H. Koivuluoto, P. Vuoristo, G. Bolelli, F. Bozza, and L. Lusvarghi, Microstructural characteristic and tribological behavior of HVOF-sprayed novel Fe-based alloy coatings, *Coatings*, 2014, **4**, p 98-120

60. M. Kašparová, F. Zahálka, Š. Houdková, and P. Ctibor, Properties of HVOF sprayed coatings influenced by laser after-treatment. in *Proceedings of International Conference MATRIB 2007*, 21-23 June 2007, Croatia. ISBN:978-953-7040-12-3

61. G. Bolelli and L. Lusvarghi, Heat treatment effects on the tribological performance of HVOF sprayed Co-Mo-Cr-Si coatings, *J. Therm. Spray Technol.*, 2006, **15**(4), p 80-810

62. G. Bolelli, V. Cannillo, L. Lusvarghi, M. Montorsi, F.B. Mantini, and M. Barletta, Microstructural and tribological comparison of HVOF-sprayed and post-treated M-Mo-Cr-Si (M=Co,Ni) alloy coatings, *Wear*, 2007, **263**, p 1397-1456

63. G. Bolelli, B. Bonferroni, J. Laurila, L.Lusvarghi, A. Milanti, K. Niemi, and P. Vuoristo, Micromechanical properties and sliding wear behavior of HVOF-sprayed FE-based alloy coatings, *Wear*, 2012, **276-277**, p 29-47